

A detailed chemical kinetic model for the combustion of gas phase ammonium nitrate

Yu-ichiro Izato^{*,**†} and Atsumi Miyake^{**}

*Graduate School of Environment and Information Sciences, Yokohama National University,
79-7 Tokiwadai, Hodogaya-ku, Yokohama-shi, Kanagawa, 240-8501 JAPAN

Phone: +81-45-339-3981

† Corresponding author: izato-yuichiro-hk@ynu.jp

**Institute of Advanced Sciences, Yokohama National University,
79-7 Tokiwadai, Hodogaya-ku, Yokohama-shi, 240-8501 JAPAN

Received: January 26, 2017 Accepted: December 8, 2017

Abstract

In this work, a mechanism for gas phase combustion of ammonium nitrate (AN) was identified and investigated. The optimized structures of reactants, products, and transition states were generated at the ω B97XD/6-311++G (d,p) level of theory and the total electron energies of such structures were calculated at the CBS-QB3 level of theory. The new kinetic model was subsequently used to predict low-pressure AN decomposition products, and the results were compared with the experimental data in the literature. Good agreement was found in terms of the concentrations of decomposition products, although the simulation predicted lower amounts of some products than were determined experimentally, suggesting that surface catalytic decomposition on the reactor walls may affect the AN decomposition process. A modified model including surface catalytic reactions provided better predictions. Detailed chemical reaction calculations were used to determine the AN ignition mechanism. During an induction period, the homolytic cleavage of HNO_3 , with a high energy barrier, initiates a chain reaction by generating $\text{OH}\cdot$ and NO_2 ; after which $\text{OH}\cdot$ attacks NH_3 to yield NH_2 . This NH_2 reacts with NO_2 to yield HONO via NH_2O . Finally, HONO attacks HNO_3 to yield $t\text{-ONONO}_2$ and this compound decomposes to start a chain-branching reaction: $t\text{-ONONO}_2 \rightarrow \text{NO}_2 + \text{NO}_2 + \text{H}_2\text{O}$. It was determined that, due to the stability of NH_3 , this species is not attacked by NO_2 but solely by $\text{OH}\cdot$. The production of $\text{OH}\cdot$ was therefore determined to be the rate-determining step for AN decomposition in the gas phase. The results of this work also demonstrate that, following sufficient accumulation of radicals, the mixture of gas phase HNO_3 and NH_3 ignites and the temperature rises sharply.

Keywords: ammonium nitrate, kinetic model, combustion, ignition mechanism, DFT

1. Introduction

Ammonium nitrate (AN) is widely used as a fertilizer and as an ingredient in industrial explosives and oxidizing chemical compositions because it is relatively cheap, releases almost 100% gaseous products upon reaction, and has a positive oxygen balance ($+20.0 \text{ g g}^{-1}$). Unfortunately, tragic accidental explosions involving AN have occurred in the past,^{2)–5)} including incidents at a West Fertilizer Company storage facility in Texas in 2013⁴⁾ and at an AZF plant in Toulouse, France, in 2001⁵⁾. To allow the safe development and use of AN-containing devices, it is

important to understand the reaction mechanisms, combustion behaviors, and thermal stabilities of AN compositions. As such, there have been many studies on the decomposition and combustion mechanisms of AN compositions^{6)–35)}.

Combustion of energetic materials, including AN, is typically characterized by a diverse range of physical and chemical processes that occur in a complex series of stages. Analyzing the behavior of an energetic material in both the condensed and gas phases is therefore an important step in obtaining a better understanding of its

combustion behavior. To understand the combustion mechanism, a detailed chemical reaction simulation is helpful, and many researchers have developed reliable reaction mechanisms for gas phase H/N/O compounds. Cagnina *et al.*²⁸⁾ and Lin and Park^{29),30)} constructed detailed kinetics models for AN decomposition and ammonium dinitramide combustion, while Daimon *et al.*³¹⁾ developed a model to simulate the species and reactions that occur during the combustion of a hypergolic $\text{N}_2\text{H}_4/\text{N}_2\text{O}_4$ mixture. Ermolin investigated the combustion mechanism of ammonium dinitramide^{32),33)} using a detailed kinetic model.

The work reported herein had several goals: firstly, to improve the previous detailed chemical model of AN combustion by identifying new reactions and providing relevant kinetic data; secondly, to validate the proposed mechanisms by comparing the predictions to the experimental data obtained by Lin *et al.*; and lastly, to simulate AN ignition behavior and to obtain a better understanding of the ignition mechanism.

2. Computational

The geometries of the reactants, products, and transition states were optimized at the $\omega\text{B97XD}/6\text{-311++G}$ (d,p) level³⁴⁾ of theory using the Gaussian 09 software package³⁵⁾. Gordon *et al.*³⁴⁾ developed the ωB97XD method, which includes empirical dispersion forces and is believed to be reliable when applied to systems with weak van der Waals forces. Their group also reported that the ωB97XD method yields satisfactory accuracy for kinetics and non-covalent interactions³⁴⁾.

During computations, transition states (TSs) were extensively searched for and, if found, an intrinsic reaction coordinate (IRC) calculation was conducted in order to assign reactants and products to the TS. The energies of the corresponding molecules were evaluated at the CBS-QB3³⁶⁾ level of theory, since this is a complete basis method with a reasonable time expense. In this study, geometries and frequencies were calculated at the $\omega\text{B97XD}/6\text{-311++G}$ (d,p) level. The optimized geometries were fixed with no changes allowed, and the energies were calculated using the CBS-QB3 method, which is considered to be a cost-effective strategy for obtaining chemically accurate thermochemical calculations.

Transition state theory (TST) calculations were also performed to obtain the rate coefficient by using the Gaussian postprocessor (GPOP) program suite³⁷⁾ developed by Miyoshi^{38)–40)}. GPOP is a collection of tools for the estimation of the thermodynamics and rate coefficients of gas-phase reactions.

The CBS-QB3 method is known to generate errors during calculations for many nitrogen-based species, leading to significant inaccuracies in the prediction of rate constants. The aim of the present work was not to obtain highly accurate rate coefficients for each reaction, but to more fully elucidate the AN ignition mechanism. We believe that calculations at this level of theory can still provide valuable insights into the combustion behavior of AN.

3. Results and discussion

3.1 Chemical kinetic modeling

3.1.1 Reaction $\text{HNO}_3 + \text{NH}_3 \rightarrow \text{NH}_2\text{NO}_2 + \text{H}_2\text{O}$

We initially identified and investigated the bimolecular reaction of NH_3 and HNO_3 , shown below. We started with the two neutral species HNO_3 and NH_3 , rather than the ionic species NO_3^- and NH_4^+ , because ionic species are not thermally favorable in the gas phase. Thus, reaction paths including ionic species were omitted from consideration as reasonable reaction paths in this study.



Figure 1 presents the potential energy profile of the reaction, including the optimized structure of the transition state (TS). This process is initiated by cleavage of the N–OH bond in HNO_3 , after which the resulting OH-abstracts a H from NH_3 (TS1), while the dissociated NO_2 combines with the dehydrogenated NH_2 to form NH_2NO_2 . The associated energy barrier was determined to be 196.3 kJ mol^{-1} at the CBS-QB3// $\omega\text{B97XD}/6\text{-311++G}$ (d,p) level of theory. The NH_2NO_2 subsequently decomposes to N_2O and H_2O . The rate coefficient for this reaction, k_{TS1} , at a given temperature T was determined using simple TST as follows:

$$k_{\text{TS1}} = 1.98 \times 10^{-1} \times T^{3.53} \exp(-22195/T) \text{ cm}^3 \text{ mol}^{-1} \text{ s}^{-1} \quad (1)$$

3.1.2 Reaction $\text{HNO}_3 + \text{HNO}_3$

Two molecules of HNO_3 may also decompose to yield N_2O_5 and H_2O as follows:



We examined this self-decomposition reaction and the subsequent processes. Figure 2 depicts the potential energy profile and optimized TS structure. The energy barrier was determined to be 89.8 kJ mol^{-1} at the CBS-QB3// $\omega\text{B97XD}/6\text{-311++G}$ (d,p) level of theory. This reaction begins with a H- transfer from one HNO_3 to the other. The resulting H_2NO_3 subsequently decomposes to H_2O and NO_2 , and NO_2 binds to NO_3 from the first HNO_3 to form N_2O_5 . The rate coefficient, k_{TS2} , for R2 was also evaluated using simple TST, as indicated below:

$$k_{\text{TS2}} = 4.14 \times 10^{-1} \times T^{3.25} \exp(-12870/T) \text{ cm}^3 \text{ mol}^{-1} \text{ s}^{-1} \quad (2)$$

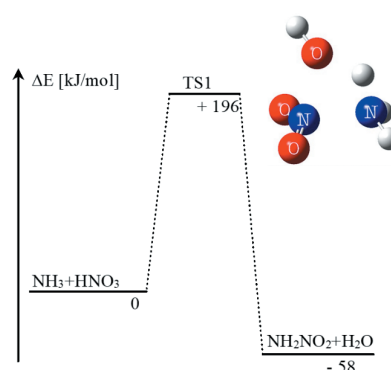


Figure 1 Potential energy profile for the bimolecular reaction $\text{NH}_3 + \text{HNO}_3 \rightarrow \text{NH}_2\text{NO}_2 + \text{H}_2\text{O}$ as calculated at the CBS-QB3// $\omega\text{B97XD}/6\text{-311++G}$ (d,p) level of theory.

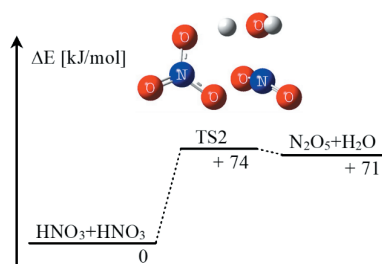


Figure 2 Potential energy profile for the bimolecular reaction $\text{HNO}_3 + \text{HNO}_3 \rightarrow \text{N}_2\text{O}_5 + \text{H}_2\text{O}$ as calculated at the CBS-QB3// ω B97XD/6-311++G(d,p) level of theory.

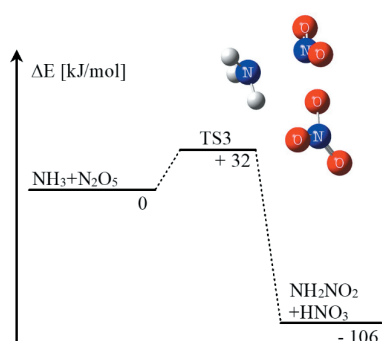


Figure 3 Potential energy profile for the bimolecular reaction $\text{NH}_3 + \text{N}_2\text{O}_5 \rightarrow \text{NH}_2\text{ONO}_2 + \text{HNO}_3$ as calculated at the CBS-QB3// ω B97XD/6-311++G(d,p) level of theory.

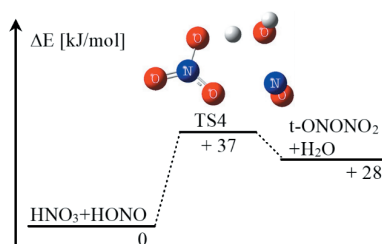


Figure 4 Potential energy profile for the bimolecular reaction $\text{HNO}_3 + \text{HONO} \rightarrow t\text{-ONONO}_2 + \text{H}_2\text{O}$ as calculated at the CBS-QB3// ω B97XD/6-311++G(d,p) level of theory.

3.1.3 Reaction $\text{NH}_3 + \text{N}_2\text{O}_5 \rightarrow \text{NH}_2\text{ONO}_2 + \text{HNO}_3$

Following the self-decomposition of HNO_3 , the resulting N_2O_5 is capable of oxidizing NH_3 , as in the reaction below.



Figure 3 shows the potential energy profile of R3 and the optimized TS structure. The energy barrier was calculated to be 27.5 kJ mol^{-1} at the CBS-QB3// ω B97XD/6-311++G(d,p) level of theory. The bimolecular reaction of N_2O_5 and NH_3 begins with the decomposition of N_2O_5 to NO_2 and NO_3 , after which NO_2 immediately combines with NH_3 to form NH_3NO_2 as TS3. The NO_3 removes a H from NH_3NO_2 to finally yield NH_2ONO_2 and HNO_3 . The rate coefficient, k_{TS3} , for R3 was determined using simple TST, as below.

$$k_{\text{TS3}} = 8.88 \times T^{2.85} \exp(-2924/T) \text{ cm}^3 \text{ mol}^{-1} \text{ s}^{-1} \quad (3)$$

3.1.4 Reaction $\text{HNO}_3 + \text{HONO} \rightarrow 2\text{NO}_2 + \text{H}_2\text{O}$

In this work, we also identified and investigated a bimolecular reaction series involving HNO_3 and HONO , as shown below.

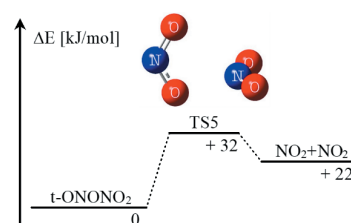


Figure 5 Potential energy profile for the reaction $t\text{-ONONO}_2 \rightarrow \text{NO}_2 + \text{NO}_2$, as calculated at the CBS-QB3// ω B97XD/6-311++G(d,p) level of theory.

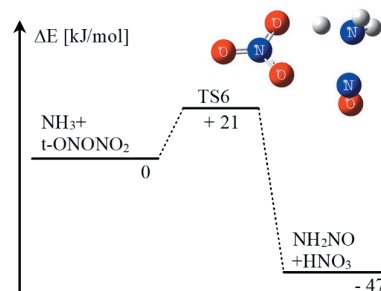


Figure 6 Potential energy profile for the bimolecular reaction $\text{NH}_3 + t\text{-ONONO}_2 \rightarrow \text{NH}_2\text{NO} + \text{HNO}_3$, as calculated at the CBS-QB3// ω B97XD/6-311++G(d,p) level of theory.

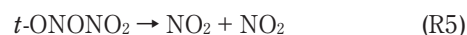


Figure 4 shows the potential energy profiles of the series of reactions, including the optimized structures of the TSs. The cleavage of the N–OH bond in HONO triggers the decomposition, after which the $\text{OH}\cdot$ abstracts a H from HNO_3 (TS4), while the dissociated $\text{NO}\cdot$ combines with NO_3 to form $t\text{-ONONO}_2$. The associated energy barrier was determined to be 36.7 kJ mol^{-1} at the CBS-QB3// ω B97XD/6-311++G(d,p) level of theory. Subsequently, the $t\text{-ONONO}_2$ decomposes to give two NO_2 molecules via TS5, as shown in Figure 5. The dissociation energy of $t\text{-ONONO}_2$ was determined to be 22 kJ mol^{-1} . The respective rate coefficients, k_{TS4} and k_{TS5} , for reactions R4 and R5 were evaluated using simple TST, as follows:

$$k_{\text{TS4}} = 2.40 \times 10^{-1} \times T^{3.47} \exp(-3595/T) \text{ cm}^3 \text{ mol}^{-1} \text{ s}^{-1} \quad (4)$$

$$k_{\text{TS5}} = 2.95 \times 10^{12} \times T^{0.17} \exp(-3975/T) \text{ s}^{-1} \quad (5)$$

3.1.5 Reaction $\text{NH}_3 + t\text{-ONONO}_2 \rightarrow \text{NH}_2\text{NO} + \text{HNO}_3$

The oxidation of NH_3 by $t\text{-ONONO}_2$ was also modeled as follows:



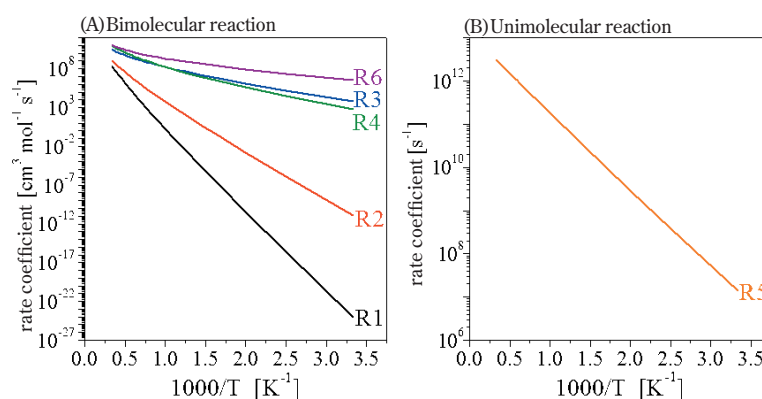
Figure 6 shows the potential energy profile of R6 and the optimized TS structure. The energy barrier was calculated to be 27.5 kJ mol^{-1} at the CBS-QB3// ω B97XD/6-311++G(d,p) level of theory. The reaction of $t\text{-ONONO}_2$ and NH_3 begins with the decomposition of $t\text{-ONONO}_2$ to $\text{NO}\cdot$ and NO_3 , after which $\text{NO}\cdot$ immediately combines with NH_3 to form $\text{NH}_3\text{NO}\cdot$ as TS6. NO_3 then removes a H from $\text{NH}_3\text{NO}\cdot$ to yield NH_2NO_2 and HNO_3 . The rate coefficient,

Table 1 Additional reactions and rate coefficients employed during the kinetic modeling of AN combustion.

No.	Reaction	ΔE_0 [kJ mol ⁻¹]		k		
		TS	Product	A^1	n	ΔE_a^2
1	$\text{NH}_3 + \text{HNO}_3 \rightleftharpoons \text{NH}_2\text{NO}_2 + \text{H}_2\text{O}$ (TS1)	196.3	-57.9	1.98×10^{-1}	3.53	184.5
2	$\text{HNO}_3 + \text{HNO}_3 \rightleftharpoons \text{N}_2\text{O}_5 + \text{H}_2\text{O}$ (TS2)	74.1	70.7	4.13×10^1	3.24	107.0
3	$\text{NH}_3 + \text{N}_2\text{O}_5 \rightleftharpoons \text{NH}_2\text{NO}_2 + \text{HNO}_3$ (TS3)	32.4	-105.6	8.88	2.85	24.3
4	$\text{HNO}_3 + \text{HONO} \rightleftharpoons t\text{-ONONO}_2 + \text{H}_2\text{O}$ (TS4)	36.7	27.9	2.40×10^{-1}	3.47	29.9
5	$t\text{-ONONO}_2 \rightleftharpoons \text{NO}_2 + \text{NO}_2$ (TS5)	32.0	22.1	2.95×10^{12}	0.17	33.1
6	$\text{NH}_3 + t\text{-ONONO}_2 \rightleftharpoons \text{NH}_2\text{NO} + \text{HNO}_3$ (TS6)	20.7	-46.9	3.14×10^1	2.79	10.7

¹ Frequency factor is given in units of cm³, mol, and s.

² Activation energy is in units kJ mol⁻¹.

**Figure 7** Rate coefficients for the (A) bimolecular and (B) unimolecular AN combustion reactions in Table 1.

k_{TS6} , for R6 was determined using simple TST, as in the following expression:

$$k_{\text{TS6}} = 3.14 \times 10^1 \times T^{2.79} \exp(-1283/T) \text{ cm}^3 \text{ mol}^{-1} \text{ s}^{-1} \quad (6)$$

3.2 Simulations

The kinetics of AN decomposition were modeled based on TST, using the parameters provided in Table 1. During this study, we modified the YNU 1.1 model previously reported by our group⁴¹. The YNU 1.1 model has been employed to analyze the decomposition of hydroxylamine in the gas phase. The majority of the elementary reactions of N-H species and the corresponding rate coefficients in this mechanism are taken from a report by Dean and Bozzelli⁴², while data for the reaction $\text{NH}_2 + \text{OH} \rightleftharpoons \text{NH}_2\text{OH}$ are from the NIST kinetics database⁴³, and data for the reaction $\text{HNO}_3 \rightleftharpoons \text{OH} + \text{NO}_2$ are from the literature²⁹. However, the subset of reactions related to hydrogen combustion in the YNU01 model was replaced by a more recently derived mechanism⁴⁴. The new model incorporates 41 species and 282 reactions. Figure 7 plots the variations in the rate coefficients of the reactions listed in Table 1 with temperature.

3.2.1 Low pressure decomposition products

To validate the model, we calculated the expected products of AN decomposition at low pressure and compared the predictions to the experimental observations of Lin *et al.*, who studied the thermal decomposition of AN in the gas phase under low-pressure

conditions over the range of 250–683 °C by pyrolysis/mass spectrometry using a reactor coated with boric acid³⁰. The CHEMKIN-PRO program suite⁴⁵ was employed for these calculations. Figure 8 plots the concentrations of AN decomposition products against the reaction temperature and shows both the simulated and experimental results.

The previous model³⁰ was insufficient to account for the consumption of NH₃ and the formation of H₂O. As can be seen in the dash-dotted lines in Figure 8, no noticeable decomposition of NH₃ was found using this model. It is known that the decomposition of HNO₃ is affected by wall surfaces through the heterogeneous decomposition reaction $\text{HNO}_3 + \text{M}(\text{wall}) \rightarrow \text{NO}_2 + \text{OH} + \text{M}(\text{wall})$, which has a reaction rate much higher than that of homogeneous decomposition at the reactor surface^{30,46}. Thus, the heterogeneous decomposition of HNO₃ was taken into consideration. In the previous study³⁰, the kinetics of the heterogeneous reaction of HNO₃ on the wall were obtained using inverse analysis. The rate was determined by varying the rate to match the modeled yields of NH₃ and H₂O to the experimentally measured concentrations. The adjusted kinetics provided excellent predictions. However, our new model did not include any such adjustment of parameters to experimental data. The dashed lines in Figure 8 show the predictions of the YNU 1.1 model with the new kinetic components described in Section 3.1. It can be seen that the data obtained from the kinetics model agreed reasonably well with the experimental results without requiring the use of any fitting parameters. We therefore conclude that the new model can provide an

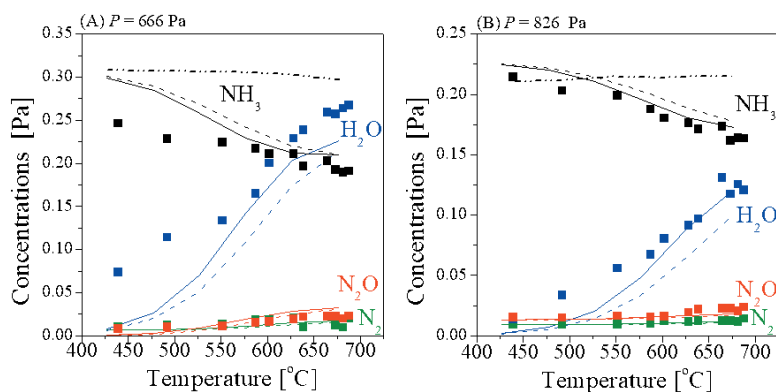


Figure 8 Comparison of experimental data and kinetic modeling results for the AN decomposition process. The square symbols and dash-dotted lines (NH_3) represent experimental data from a literature report³⁰⁾. The plots were obtained using the modified YNU 1.1 model (dashed lines) and the YNU01 model including the heterogeneous decomposition of HNO_3 on the reactor walls (solid lines). Initial conditions were: (A) $\text{NH}_3 = \text{HNO}_3 = 3.1 \times 10^{-1}$ Pa, $\text{N}_2 = 9.3 \times 10^{-1}$ Pa, reaction time = $23.16 T^{-1}$ s (T in kelvin), and $P = 666.6$ Pa (using He), and (B) $\text{NH}_3 = \text{HNO}_3 = 2.3 \times 10^{-1}$ Pa, $\text{N}_2 = 9.3 \times 10^{-1}$ Pa, $\text{N}_2\text{O} = 13.3 \times 10^{-1}$ Pa, reaction time = $15.16 T^{-1}$ s, and $P = 826$ Pa (using He).

improved understanding of the decomposition of AN. It is evident, however, that the simulations using our new model predict that less NH_3 will be consumed and less H_2O will be generated compared to the experimental observations. H_2O is primarily generated from the reactions $\text{HNO}_3 \rightarrow \text{NO}_2 + \text{OH}\cdot$ and $\text{NH}_3 + \text{OH}\cdot \rightarrow \text{NH}_2\cdot + \text{H}_2\text{O}$. The homogeneous decomposition reaction $\text{HNO}_3 \rightarrow \text{NO}_2 + \text{OH}\cdot$ is too slow to initiate a chain reaction. We also calculated the reaction coefficient for the heterogeneous decomposition reaction in a glass reactor (140 mm length) based on a literature report⁴⁶⁾ as follows:

$$k' = 1.89 \times 10^1 \times T^{2.12} \exp(-11490/T) \text{ s}^{-1} \quad (7)$$

The solid lines in Figure 8 indicate the predicted concentrations using the new model when incorporating heterogeneous decomposition. When modified in this manner, the model provides better predictions. However, further improvement is needed to provide better prediction at temperatures below approximately 550 °C. The decomposition rate was significantly dependent on the surface-to-volume ratio and insensitive to temperature. Therefore, in order to improve the accuracy of the predictions, we should obtain and determine kinetics for each reactor.

3.2.2 Ignition mechanism

To obtain a better understanding of the AN ignition process, the modified YNU 1.1 model was used to calculate the ignition delay time of a 1:1 (on a molar basis) NH_3/HNO_3 gas mixture at $P_0 = 1$ atm and $T_0 = 350$ °C during adiabatic combustion (meaning constant enthalpy and pressure). These calculations were performed using the CHEMKIN-PRO program suite⁴⁵⁾. The T_0 value of 350 °C was chosen because this temperature is approximately the dissociation point of AN at 1 atm⁷⁾.

The temperature and species time profiles for an initial temperature of $T_0 = 350$ °C are shown in Figure 9, in which the abrupt rise in temperature at approximately 0.15 s clearly indicates the ignition. During the induction period, the concentrations of NO_2 , HONO, and $\text{OH}\cdot$ are all seen to increase.

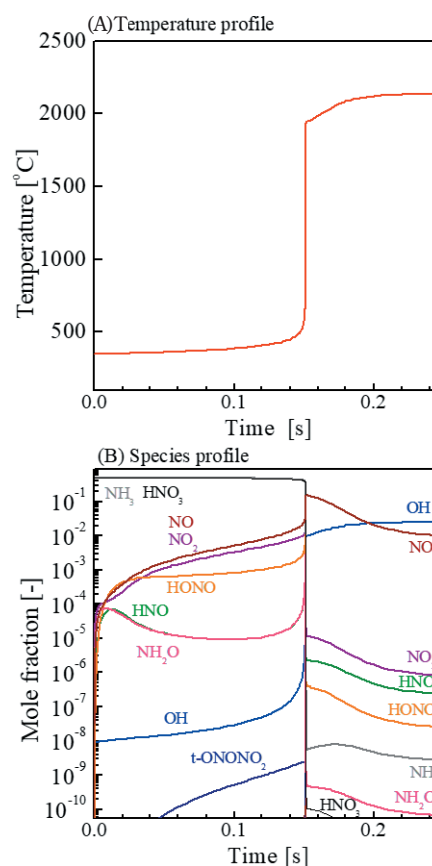


Figure 9 Temperature (A) and species (B) time histories for a 1:1 molar mixture of gaseous HNO_3/NH_3 at $P_0 = 1$ atm and $T_0 = 350$ °C under adiabatic constant pressure conditions.

Figure 10 summarizes the absolute production rates of important species (NH_3 , HNO_3 , NO_2 , HONO, and NH_2O), calculated based on a reaction path analysis using the CHEMKIN-PRO program suite⁴⁵⁾. The majority of the HNO_3 is consumed by two reactions: $\text{HNO}_3 \rightarrow \text{NO}_2 + \text{OH}\cdot$ and $\text{HNO}_3 + \text{HONO} \rightarrow t\text{-ONONO}_2 + \text{H}_2\text{O}$. Because NH_3 is relatively stable, it reacts to yield $\text{NH}_2\cdot$ via the attack of $\text{OH}\cdot$ rather than NO_2 . However, NO_2 can react with $\text{NH}_2\cdot$ to yield $\text{NH}_2\text{O}\cdot$ and HNO. The majority of NO_2 is consumed by three reactions: $\text{NH}_2\cdot + \text{NO}_2 \rightarrow \text{NH}_2\text{O}\cdot + \text{NO}$, $\text{HNO} + \text{NO}_2 \rightarrow \text{NO}\cdot + \text{HONO}$, and $\text{NH}_2\text{O}\cdot + \text{NO}_2 \rightarrow$

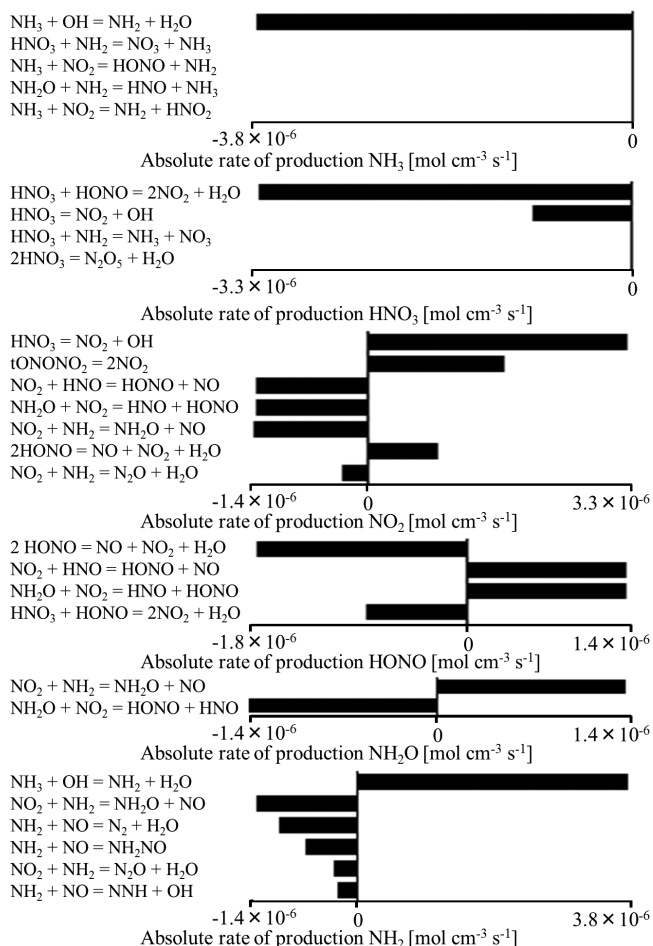


Figure 10 Absolute rates of production of important species (NH_3 , HNO_3 , NO_2 , HONO and NH_2O) at 0.15 s and $T_{0.15} = 383^\circ\text{C}$, calculated using the modified YNU01 model using CHEMKIN-PRO.

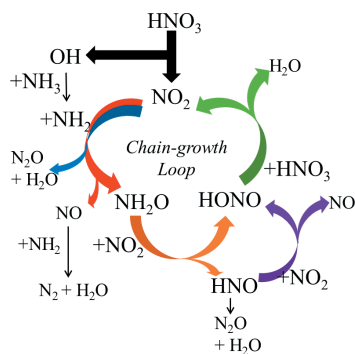


Figure 11 A reaction scheme for AN decomposition during the induction period.

$\text{HNO} + \text{HONO}$. The HONO promotes the decomposition of HNO_3 to yield two NO_2 via $t\text{-ONONO}_2$. Figure 11 depicts the proposed AN ignition mechanism based on these results. The homolytic cleavage of HNO_3 , $\text{HNO}_3 \rightarrow \text{OH} + \text{NO}_2$, triggers the chain reaction in which OH reacts with NH_3 to give NH_2 and H_2O . The reaction of $\cdot\text{NH}_2$ and $\cdot\text{NO}_2$ has two possible paths, yielding either N_2O and H_2O or NH_2O and HNO . NO_2 attacks NH_2O or HNO to yield either HNO and HONO , or HONO and NO , respectively, after which HONO attacks HNO_3 to yield two NO_2 and H_2O via $t\text{-ONONO}_2$. This chain-propagation loop increases the NO_2 and HONO concentrations and prolongs the radical chain reaction. As noted, the stability of NH_3

prevents its reaction with the low-reactivity NO_2 radical. Thus, the production of the high-reactivity OH radical via the homolytic cleavage of HNO_3 is the rate-determining step for AN decomposition in the gas phase. In this proposed process, the accumulation of a sufficient concentration of radical species leads to ignition of the HNO_3 and NH_3 gas mixture with an attendant rapid temperature rise.

4. Conclusions

The combustion pathway of AN in the gas phase was investigated on the basis of quantum chemical calculations. The calculations were performed at the $\omega\text{B97XD}/6\text{-311}++\text{G}(\text{d,p})$ and $\text{CBS-QB3}/\omega\text{B97XD}/6\text{-311}++\text{G}(\text{d,p})$ levels of theory. Mechanisms for the reactions $\text{HNO}_3 + \text{NH}_3 \rightarrow \text{NH}_2\text{NO}_2 + \text{H}_2\text{O}$; $\text{HNO}_3 + \text{HNO}_3 \rightarrow \text{N}_2\text{O}_5 + \text{H}_2\text{O}$; $\text{N}_2\text{O}_5 + \text{NH}_3 \rightarrow \text{NH}_2\text{NO}_2 + \text{H}_2\text{O}$; $\text{HNO}_3 + \text{HONO} \rightarrow t\text{-ONONO}_2 + \text{H}_2\text{O}$; $t\text{-ONONO}_2 \rightarrow \text{NO}_2 + \text{NO}_2$; and $t\text{-ONONO}_2 + \text{NH}_3 \rightarrow \text{NH}_2\text{NO}_2 + \text{HNO}_3$ were developed and added to the YNU01 model⁽⁴¹⁾. To validate the modified mechanisms, we compared the predicted products of the thermal decomposition of gas-phase AN to experimental data. The kinetics model data agree reasonably well with the experimental results without the use of any fitting parameters. The new model should, however, be modified to incorporate heterogeneous decomposition at the reactor walls. A model revised in this manner will be able to provide better predictions of AN decomposition in a reactor. Detailed chemical reaction simulations revealed that the ignition occurs after an induction period at an initial temperature of 350°C , which is the dissociation point of AN at 1 atm. Homolytic HNO_3 cleavage, $\text{HNO}_3 \rightarrow \text{NO}_2 + \text{OH}$, starts the decomposition reaction, and then OH attacks NH_3 to yield NH_2 . NO_2 does not attack NH_3 because NH_3 is stable, but it reacts with NH_2 to yield NH_2O . NH_2O reacts with NO_2 to yield HONO and HNO . HONO attacks HNO_3 according to the reaction $\text{HNO}_3 + \text{HONO} \rightarrow 2\text{NO}_2 + \text{H}_2\text{O}$, which is a chain-branching process. Due to the stability of NH_3 , only OH can attack this unreactive species. The production of OH , which occurs via the homolytic cleavage of HNO_3 , is the rate-determining step of AN decomposition in the gas phase. After sufficient radical accumulation, the HNO_3 and NH_3 gas mixture ignites and the temperature rises sharply.

References

- 1) C. Oommen and S. R. Jain, *J. Hazard. Mater.*, A67, 253–181 (1999).
- 2) J. C. Oxley, J. L. Smith, E. Rogers, and M. Yu, *Thermochemica Acta.*, 384, 23–45 (2002).
- 3) G. Marlair and M. Kordek, *J. Hazard. Mater.*, A123, 13–28 (2005).
- 4) Chemical Safety Board, "Preliminary Findings of the U.S. Chemical Safety Board from its Investigation of the West Fertilizer Explosion and Fire", <http://www.csb.gov/assets/1/19/West_Preliminary_Findings.pdf> (accessed: 15–January–2013). (online).
- 5) N. Dechy, T. Bourdeaux, A. Ayrault, M. Kordek, and J. L. Coze, *J. Hazard. Mater.*, 111, 131–138 (2004).
- 6) V. P. Sinditskii, V. Y. Egorshv, A. Y. Levshenkov, and V. V. Serushkin, *Propellants Explos. Pyrotech.*, 30, 269–280 (2005).
- 7) V. P. Sinditskii, V. Y. Egorshv, V. V. Serushkin, and S. A. Filatov, *Combust Expl Shock Waves.*, 48, 81–99 (2012).
- 8) K. Kajiyama, Y. Izato, and A. Miyake, *J. Therm. Anal. Calorim.*, 113,

- 1475–1480 (2013).
- 9) Y. Izato, A. Miyake, and S. Date, *Prop. Explos. Pyrotechnics*, 38, 129–135 (2013).
- 10) A. Miyake and Y. Izato, *Intl. J. Energetic Materials and Chemical Propulsion*, 9, 523–531 (2011).
- 11) Y. Izato, H. Echigoya, and A. Miyake, *Sci. Tech. Energetic Materials*, 70, 101–104 (2009).
- 12) Y. Izato, K. Kajiyama, and A. Miyake, *Sci. Tech. Energetic Materials*, 75, 128–133 (2014).
- 13) J. C. Oxley, J. L. Smith, and W. Wang, *J. Phys. Chem.*, 98, 3901–3907 (1994).
- 14) K. R. Brower, J. C. Oxley, and M. Tewari, *J. Phys. Chem.*, 89, 4029–4033 (1989).
- 15) G. B. Manelis, G. M. Nazin, Y. I. Rubtsov, and V. A. Strunin, “Thermal Decomposition and Combustion of Explosives and Propellants” Taylor & Francis, 175–187 (2003).
- 16) Y. Wada and M. Arai, *Sci. Tech. Energetic Materials*, 71, 39–43 (2010).
- 17) Y. Miyata and K. Hasue, *J. Energ. Mater.*, 29, 344–359 (2011).
- 18) M. Pandey, S. Jha, R. Kumar, S. Mishra, and R. R. Jha, *J. Therm. Anal. Calorim.*, 107, 135–140 (2012).
- 19) A. G. Keenan, K. Notz, and N. B. Franco, *J. Am. Chem. Soc.*, 91, 3168–3171 (1969).
- 20) J. H. Macneil, H. Zhang, P. Berseth, and W. C. Trogler, *J. Am. Chem. Soc.*, 119, 9738–9744 (1997).
- 21) X. R. Li and H. Koseki, *Process Safety and Environmental Protection*, 83, B1, 31–37 (2005).
- 22) J. Sun, Z. Sun, Q. Wang, H. Ding, T. Wang, and C. Jiang, *J. Hazard. Mater.*, B127, 204–210 (2005).
- 23) J. C. Oxley, J. L. Smith, S. Naik, and J. Moran, *J. Energe. Mater.*, 27, 17–39 (2009).
- 24) V. A. Koroban, *Propellants Explos. Pyrotech.*, 19, 307–310 (1994).
- 25) D. G. Patil, S. R. Jain, and T. B. Brill, *Propellants Explos. Pyrotech.*, 17, 99–105 (1992).
- 26) A. Mirvakili, F. Samimi, and A. Jahanmiri, *J. Ind. Eng. Chem.*, 20, 2452–2462 (2014).
- 27) S. A. Skarlis, A. Nicolle, D. Berthout, C. Dujardin, and P. Granger, *Thermochimica Acta.*, 584, 58–66 (2014).
- 28) S. Cagnina, P. Rotureau, G. Fayet, and C. Adamo, *Phys. Chem. Chem. Phys.*, 15, 10849–10859 (2013).
- 29) J. Park, D. Chacraborty, and M. C. Lin, *Symp. (Int.) on Combust.*, 27, 2351–2357 (1998).
- 30) J. Park and M. C. Lin, *J. Phys. Chem. A*, 113, 13556–13561 (2009).
- 31) Y. Daimon, H. Terashima, and M. Koshi, *J. Propul. Power*, 30, 707–716 (2014).
- 32) N. E. Ermolin, *Combust. Explos. Shock Waves*, 40, 92–109. (2004).
- 33) N. E. Ermolin, *Combust. Explos. Shock Waves*, 43, 549–561 (2007).
- 34) J. D. Chai and M. Head-Gordon, *Phys. Chem. Chem. Phys.*, 10, 6615–6620 (2008).
- 35) M. J. Frisch, G. W. Trucks, H. B. Schlegel, G. E. Scuseria, M. A. Robb, J. R. Cheeseman, G. Scalmani, V. Barone, B. Mennucci, G. A. Petersson, H. Nakatsuji, M. Caricato, X. Li, H. P. Hratchian, A. F. Izmaylov, J. Bloino, G. Zheng, J. L. Sonnenberg, M. Hada, M. Ehara, K. Toyota, R. Fukuda, J. Hasegawa, M. Ishida, T. Nakajima, Y. Honda, O. Kitao, H. Nakai, T. Vreven, J. A. Montgomery, J. E. Peralta, F. Ogliaro, M. Bearpark, J. J. Heyd, E. Brothers, K. N. Kudin, V. N. Staroverov, T. Keith, R. Kobayashi, J. Normand, K. Raghavachari, A. Rendell, J. C. Burant, S. S. Iyengar, J. Tomasi, M. Cossi, N. Rega, J. M. Millam, M. Klene, J. E. Knox, J. B. Cross, V. Bakken, C. Adamo, J. Jaramillo, R. Gomperts, R. E. Stratmann, O. Yazyev, A. J. Austin, R. Cammi, C. Pomelli, J. W. Ochterski, R. L. Martin, K. Morokuma, V. G. Zakrzewski, G. A. Voth, P. Salvador, J. J. Dannenberg, S. Dapprich, A. D. Daniels, O. Farkas, J. B. Foresman, J. V. Ortiz, J. Cioslowski, and D. J. Fox, *Gaussian 09, Revision D.01*, Gaussian, Inc., Wallingford CT (2010).
- 36) J. A. Montgomery, M. J. Frisch, J. W. Ochterski, and G. A. Petersson, *J. Chem. Phys.*, 110, 2822–2827 (1999).
- 37) A. Miyoshi, GPOP software, rev. 2013.07.15 m5, available from the author. See <http://www.frad.t.u-tokyo.ac.jp/~miyoshi/gpop/>.
- 38) A. Miyoshi, *International Journal of Chemical Kinetics*, 42, 273–288 (2010).
- 39) A. Miyoshi, *J. Phys. Chem. A*, 115, 3301–3325 (2011).
- 40) A. Miyoshi, *International Journal of Chemical Kinetics*, 44, 59–74 (2012).
- 41) Y. Izato, M. Koshi, and A. Miyake, *Sci. Tech. Energetic Materials*, 78, 12–18 (2017).
- 42) A. M. Dean, J. W. Bozzelli, and W. C. Gardiner Jr ed., “Gas-Phase Combustion Chemistry”, 125–316, Springer-Verlag, New York (2000).
- 43) NIST Chemical Kinetics Database, Standard Reference Database 17, Version 7.0 (Web Version), Release 1.6.8 Data Version 2015.12 (accessed : 28-July-2016). (online).
- 44) K. Shimizu, A. Hibi, M. Koshi, Y. Morii, and N. Tsuboi, *J. Propul. Power*, 27, 383–395 (2011).
- 45) CHEMKIN–Pro Input Manual PRO–INP–15092–UG–1, Reaction Design, San Diego, CA (2011).
- 46) H. S. Johnston, L. Foering, Y. S. Tao, and G. H. Messerly, *J. Am. Chem. Soc.*, 73, 2319–2321 (1951).